Received: 21 December 2017 | Revised: 27 May 2018 | Accepted: 3 September 2018

DOI: 10.1111/str.12300

FULL PAPER

WILEY strain

Impact of motion blur on stereo-digital image correlation with the focus on a drone-carried stereo rig

R. Balcaen[1] | A. Lavatelli[2] | C. Jiménez-Peña[1] | H. Pfeiffer[3] | E. Zappa[2] | D. Debruyne[1]

[1]Department of Materials Engineering, KU Leuven, Ghent, Belgium

[2]Department of Mechanical Engineering, Politecnico di Milano, Milan, Italy

[3]Structural Composites and Alloys, Integrity and Nondestructive Testing, KU Leuven, Leuven, Belgium

Correspondence
Balcaen R., Department of Materials Engineering, KU Leuven, Campus Gent, Gebroeders De Smetstraat 1, 9000 Ghent, Belgium.
Email: ruben.balcaen@kuleuven.be

Abstract

Stereo-digital image correlation (DIC) is a wide-spread technique in the field of experimental mechanics for measuring shape, motion, and deformation and it is frequently used for material identification by using inverse methods (e.g., virtual fields method and finite element model updating). New applications emerge due to the reached maturity level of the technique, which poses new challenges towards reaching a desired level of accuracy in operating conditions. In this work, the possibility of a drone carrying an in-house-made portable DIC setup is explored, and the effect of the drone-induced vibrations on the accuracy of stereo-DIC for shape and strain measurement is evaluated. During acquisition, the relative motion between the camera system and the measured item generates motion-blurred images. The effect of this phenomenon on the precision of stereo-DIC is further evaluated in this paper.

KEYWORDS

digital image correlation, drone, feasibility study, uncertainty quantification

1 | INTRODUCTION

Stereo-digital image correlation (stereo-DIC)[1,2] has gained more and more interest in the past few years due to dropping prices of cameras and computers, leading to a significant rise in uncertainty quantification papers (e.g., Rossi & Pierron, 2012; Bornert et al., 2009; Wang, Sutton, Ke, Schreier, Reu, & Miller, 2011; Ke, Schreier, Sutton, & Wang, 2011[3–6]). As with every novel technique, the amount of published works appear in a bell-shaped curve, in which a steady increase of papers indicates the gaining maturity of the technique. If one looks at the number of stereo-DIC publications, it is clear that the technique has reached the maximum of this bell curve, leading to acceptance of the technique by industry and the development of new products. A portable stereo-DIC setup by Dantec[7] is a good example of this; it partially solves the time-consuming part of DIC by eliminating the setup and calibration time; however, the handheld device introduces new questions towards uncertainty quantification. This is mainly due to the fact that DIC was always used on a stationary setup, thus removing possible errors due to motion blur or other effects caused by setup motion,[8,9] and the fact that camera heating (e.g., Qinwai & Shaopeng, 2013[10]) could introduce errors in the precalibrated setup. A portable setup would additionally allow measurements on a reasonably stable transport system, such as multirotor drones or a generic unmanned aerial vehicle (UAV—e.g., for applications where accessibility is an issue). Up to now, one successful test of drone-based DIC can be found in literature, which is dedicated to Structural Health Monitoring.[11] In Reagan, Sabato, and Niezrecki,[11] the author clearly showed that the uncertainty of UAV-operated DIC is higher than the one of static DIC, mainly due to motion blur and poor light management. Nonetheless, the author documented the reconstruction of strain fields of a cracked bridge in operating conditions by avoiding motion blur (with a limited exposure time), which required him to acquire images in very sunny conditions. The

structure is however hardly uniformly illuminated by the sunlight, hence, the difficulties in finding a correct trade off. At the same time it is proposed to operate during night so that the experimenter can apply homogeneous and strong lighting systems, thus adding complexity and removing the flexibility of a system designed to operate in difficult to reach environments. In any case, the literature shows that avoiding motion blur with a UAV-based DIC system can be hard or almost impossible. Conversely, the present study will investigate the feasibility of mounting a stereo-DIC setup on a drone by taking the inevitability of motion blur into account. In other words, the aim is first to evaluate what errors are generated by motion blur in normal operating conditions, so that a correct uncertainty budget can be formulated for the UAV-operated DIC. Secondly, a mathematical model of motion blur will provide tools to evaluate the sensitivity of stereo-DIC in regards to the level of vibration and the exposure time.

The focus in the first part of this paper is the shape measurements of mechanical parts, which is followed by strain measurements. Since shape measurements do not require a fixed pattern on the object surface, the pattern can be projected with a portable beamer for the shape identification section. A beamer is also preferred since homogeneous lighting conditions can be created (since the projected pattern has a bright background). Experimental tests must first indicate whether the drone-induced vibrations are harmful towards shape and strain measurements. This is investigated by acquiring and analysing drone motions and imposing these on a basic stereo-DIC setup by using an electromagnetic shaker, which is able to impose a given displacement and acceleration at a specific frequency. An uncertainty quantification study on the influence of the shaking DIC system on shape and strain reconstruction is then performed by modifying the shaking frequency and the imposed accelerations. A bias was observed during this study, which could be potentially induced by motion blur in the images. Motion blur was consequentially simulated, and the introduced bias hereof was investigated and explained.

2 | EXPERIMENTAL SETUP FOR DRONE AND SHAKER TESTS

In this section, the experimental setup will be presented in this section together with all the procedures designed to assess the accuracy of UAV-based DIC. First, the drone-based DIC apparatus will be presented, together with the necessary procedures to characterise the motion of the UAV. This will provide data about the vibration patterns to be imposed by an electromagnetic shaker in the laboratory tests.

2.1 | Drone operations and vibration characterisation

The UAV stereo-DIC setup under analysis is composed by a commercially available AeroQuad quadcopter that is supposed to carry an airborne stereo vision rig. The flight program consists of a takeoff, followed by a hovering phase at an approximated height of 2.5 m in an indoor environment (thus mitigating unwanted external effects such as sudden gusts of wind). A payload of one camera (non-machinevision) was attached to increase the weight of the system. Obviously, only the hovering phase is relevant to the DIC image acquisition: The drone altitude and position should allow full coverage of the mechanical specimen within the field of view of the cameras. As for any kind of rotorcraft aerial vehicle, the hovering flight is far from being still in the vertical direction.[12] The mutual action of gravity, downwash, and ground effects generate steady and nonlinear oscillations,[13] often bounded by a limited cycle. This phenomenon is even more relevant in quadrotor configurations, since each propeller may work with a different angle of attack due to the angular velocity of the centre of mass. Given that hovering vibrations are not avoidable and, generally speaking, hardly predictable due to the nonlinear stochastic nature of the problem (small changes in initial and boundary conditions are able to generate big changes in the vibration patterns), it is of utmost importance to characterise them experimentally. In this way, they can correctly be replicated in laboratory conditions to allow a feasibility analysis. The motion of the UAV has been measured using the internal inertial measurement unit (IMU) that is usually exploited for the altitude and flight control. Data have been logged with the freely available *Blackbox Explorer* software,[14] released under the General Public Licence version 3 (GPLv3) licence. *Blackbox Explorer* has been designed with the focus on tuning the proportional-integral-derivative control of quadcopters to ensure a more stable flight by logging the accelerometers, gyroscope, stick movements, and power generated by the motors. IMU data are logged primarily by the drone microcontroller unit (MCU); then, they are transmitted to the logging computer. The operation however is not straightforward since the generic drone MCU is not capable of hard real-time operations. This results in sparsely sampled data, with an average sampling interval of 500 and a standard deviation of about 100. This is problematic, since data has to be sampled at a regular frequency to perform frequency domain analysis. Hence, the drone data have been resampled using a polyphase

filter interpolant.[15] This operation is legitimate since polyphase filters preserve information content, even though some ripples can be generated around the Nyquist frequency. This rippling phenomenon however does not affect the accuracy of the procedure since the rigid-body dynamics of the drone are located at low frequencies. The last step consists in recovering the vibration in the reference frame. In fact, the IMU is solidal to the drone local reference axis that may rotate during flight. Another issue is that microelectromechanical accelerometers suffer from heavy signal direct current (DC) drift during the flight phase. A simple Kalman filter approach however allowed to recover the vertical acceleration from IMU flight data. The hovering phase was recorded for 30 seconds and then, the power spectral density (PSD) of the acceleration channels is computed using the well-known Welch method. The results of the procedure are displayed in Figure 1, where it is possible to highlight the following issues:

- In the 0–5 band (where the rigid-body motion of the drone is expected), the z-axis acceleration is about one order in magnitude larger as compared with the other two axes. Hence, the feasibility study should concentrate on analysing the effects of vertical vibrations, considering that the other components are negligible.
- Starting from 8 Hz, all the three axes display almost the same frequency constant power density. This clear plateau is due to both noise and random uniform vibrations due to local turbulence.

With the same state observer, it is possible to retrieve data about the velocity of the drone (Figure 2). Velocity causes motion blur, which is an important indicator for this feasibility study. The plots in Figure 2 show that the vertical motion is affected by random fluctuation peaks that appear without any apparent periodicity. This feature is in line with the generic models of rotorcrafts flight dynamics, especially considering that the timing given by the propeller revolution is at much higher frequency than the rigid-body motion eigenfrequencies. By looking at the PSD of velocity in Figure 3, it is possible to find an oscillation peak at around 1.1 Hz, probably denoting the presence of a stable pole of the rigid-body motion. As for the acceleration PSDs, the contribution of the vertical axis to the overall vibration level is the most relevant one.

It is clear from Figures 1 and 3 that most vibrations are present in the vertical direction (z axis), with an exponentially decreasing acceleration spectral density of 8×10^{-2} to 2×10^{-4} $m^2 s^{-4}$ Hz^{-1} (after the steady state). The lower frequencies indicate the slow up- and down moving of the quadcopter caused by the operator trying to keep the drone at a constant height. These lower frequency components will not affect DIC measurements since they can be removed as rigid-body motion and they will not introduce motion blur due to the low exposure time of the cameras (the shutter time was set to 7.5 ms). The root mean square values of acceleration are 0.3 m s^{-2} for the vertical axis and about 0.08 m s^{-2} for the horizontal ones. This confirms that vibrations in the horizontal plane (x-axis and y-axis) are practically negligible for this setup. The maximum vertical acceleration acquired during hovering is 1.28 m s^{-2}, which was rounded off to 0.125 for the analysis of the feasibility of the drone DIC setup.

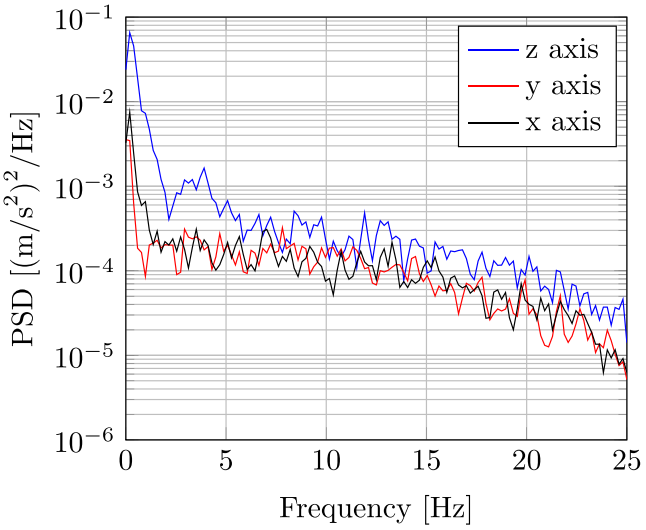

FIGURE 1 Power spectral density of acceleration along the three flight axes

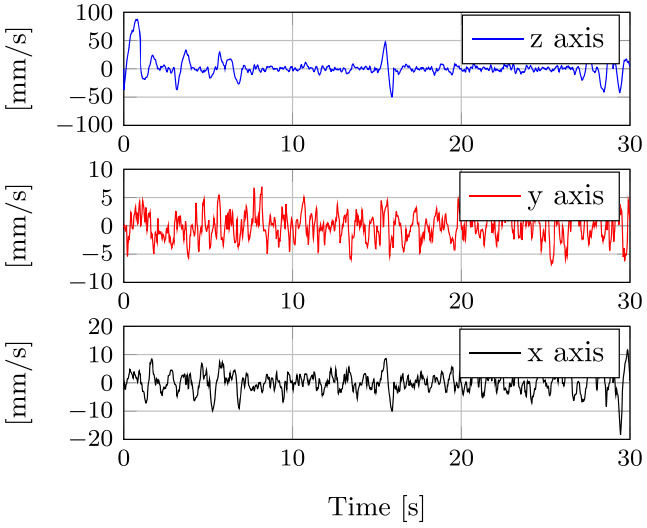

FIGURE 2 Velocity of the centre of gravity of the drone on three axes

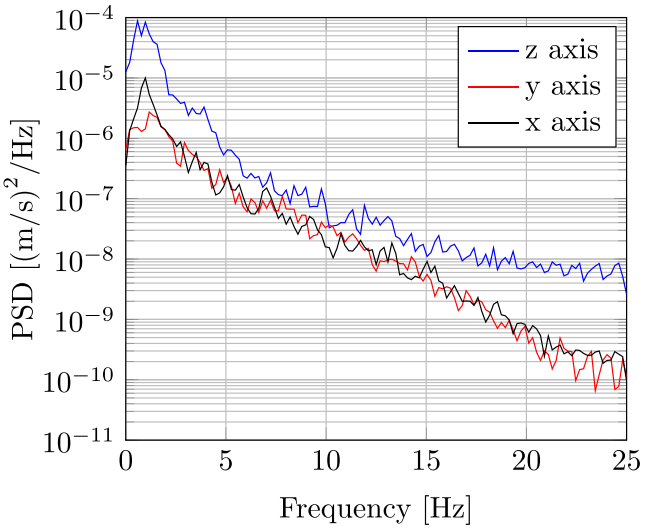

FIGURE 3 Power spectral density of velocity along the three flight axes

2.2 | Shaker operations and imposed motion

The accelerations measured during the hovering phase of the drone are imposed on a stereo-DIC setup with a *Data Physics* gravitational wave (GW)-V55 electromagnetic shaker in combination with a GW-PA300E amplifier,[16] of which the specifications are given in Table 1. Note that these specifications indicate the best possible achievable performance of the shaker (indicated as a dashed black line in Figure 4) and that the load will decrease the workability region, as

TABLE 1 Shaker specifications (gravitational wave [GW]-V55)

Specification	Value
Minimum frequency, Hz	2
Maximum frequency, Hz	8000
Rated peak force, N	311.4
Maximum rated travel, mm PtP	12.7
Maximum velocity, m s^{-1} PtP	1.1
Maximum acceleration, g	21

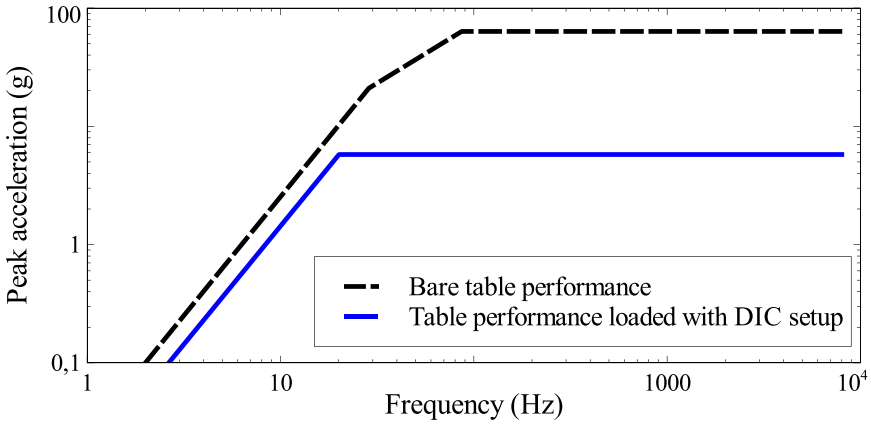

FIGURE 4 Shaker performance

indicated in Figure 4 by the blue line, depending on the load either the maximum displacement, speed, or acceleration limit will be reached, limiting the working spectrum. The maximum displacement limit was in this case the limiting factor, resulting in a limited maximum acceleration of 5.77 g, which is sufficient for the targeted application.

The natural frequency of the initial DIC setup, showed in Figure 5, was calculated before actually investigating the influence of camera vibration on shape and strain measurement, so effects induced by resonance could be excluded. A finite elements analysis, performed with Abaqus,[17] estimates that the lowest natural frequency of our setup is 661 Hz, thus far away from the frequency band of the drone-induced vibrations. Relative camera motion was also investigated before starting the actual research since it may affect significantly stereo-DIC results (as previously noted in Balcaen, Reu, Lava, & Debruyne, 2017[18] by Balcaen et al.). Accelerations of 0.125 g were imposed on the setup at a frequency range of 0–20 Hz, with steps of 5 Hz. The shaker was halted after vibrating for 2 min at a specific frequency, and 75 calibration images were taken (as suggested by Reu et al. in Reu, 2013[19]) in order to evaluate whether relative camera motion was present or not by recalibrating the stereo rig. The dashed line in Figure 6 reveals that the relative angle between cameras increased from 13.78° to 14.40° during the five vibration tests. This increase is notably higher than the expected calibration error according to Reu (2013),[19] and it will impact the shape and strain measurements. This problem was alleviated by bolting the cameras directly onto a stiff aluminium profile and bolting the profile onto the electromagnetic shaker, so relative camera motion is prohibited. The reliability of the new setup was tested by vibrating the setup again at 0.125 g, however, now, with a frequency interval from 5 to 17.5 Hz with steps of 2.5 Hz. The blue line in Figure 6 indicates that the rig had less relative camera motion, with a more monotonous behaviour and a standard deviation of 0.05°. The modified setup proved to be more stable, so it was employed for further investigation of the impact of a vibrating DIC setup on the shape and strain identification.

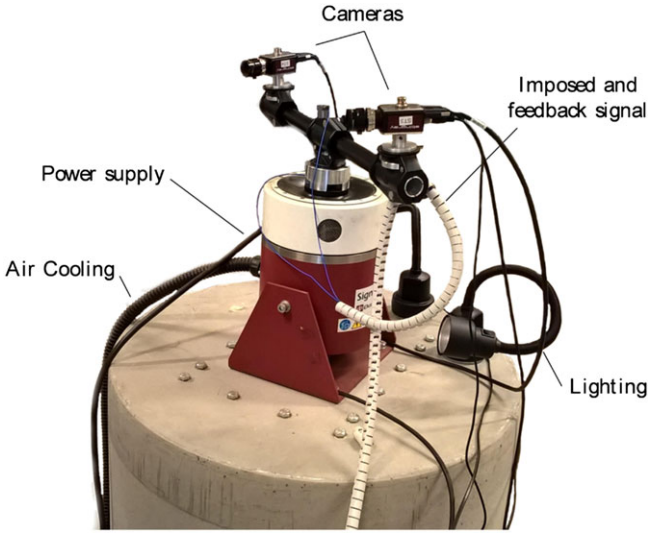

FIGURE 5 Initial setup

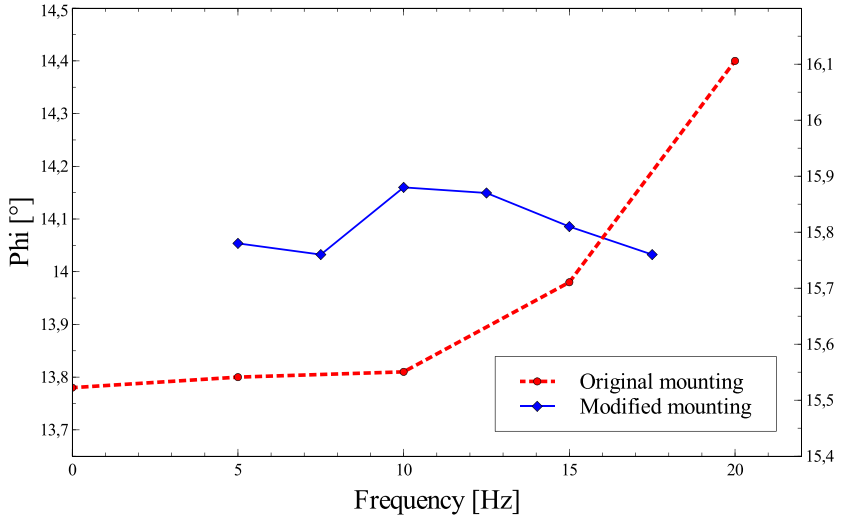

FIGURE 6 Influence of camera mounting on relative camera motion

3 | INFLUENCE ON SHAPE RECONSTRUCTION

The main goal of a portable DIC setup is the measurement of shapes, so deficiencies in structures can be identified. A good example of this is dent identification for fuselage panels in airplanes. Since fuselage panels are often damaged by bird strikes or collisions with luggage belts, a portable DIC setup could be a viable measurement tool for identifying the dent depth. Especially, a fully wireless system on a drone could be very efficient since it would decrease the amount of manual work and increase the accuracy of identified dents, since the evaluation is mainly done manually (although some automated tools or extensive tools are reported in the literature[20,21]). In any case, monitoring fuselage dents is an activity of key importance for airline operation, since denting may decrease fatigue life of aeronautic aluminium alloys up to 20%, as demonstrated in Guijt, Hill, Rausch, and Fawaz (2005).[22] The feasibility of this application is tested by measuring dents on a fuselage panel (shown in Figure 7) with the earlier mentioned setup on the electromagnetic shaker. The panel was indented at four different locations with different impact energies, and one or multiple impacts were introduced at the same location (as indicated in Table 2). These impacts were measured under different shaker conditions by projecting a speckle pattern onto the specimen. The projector was standing still on a platform isolated from shaker vibration. Consequently, the projected speckle pattern could be considered as solidly attached to the surface. The influence of shaker frequency, acceleration, and the required number of images was investigated. One reference image pair was taken with a static setup, followed by 50 image pairs while shaking the setup at a desired frequency and acceleration. The images were taken manually at random intervals so that no interference of the shaker frequency nor the acquisition frequency could be present. The same reference image and settings (i.e., subset size, step size, and initial subset location as given in Table 3) were applied to analyse each of the 50 images in such a way that the exact

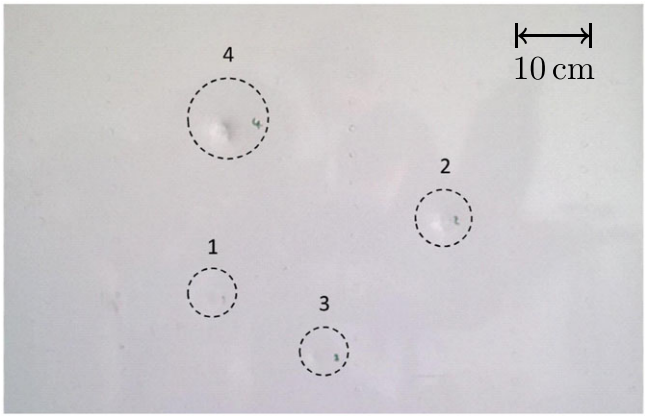

FIGURE 7 Fuselage panel for dent identification with shaking camera system

TABLE 2 Overview of impacts on fuselage panel

Dent ID	Impacts	Impact energy (J)
1	1	4
2	4	10
3	1	10
4	10	10

TABLE 3 Digital image correlation properties for the shape measurements

Parameter	Value
Camera resolution, pixels	1624 × 1234
Exposure time, μs	12,500
Camera noise level, % dynamic range	0.5
Subset size, pixels	45
Step, pixels	3
Interpolation	B spline
Transformation	Affine
Average speckle size, pixels	8
Average speckle spacing, pixels	6

same points were evaluated for every measurement. That is, by using the same reference image and changing images of the "deformed state" (caused by the shaking camera system), the same positions can be tracked over time. Rigid-body removal was applied on all results, and only the data of the 50 images were taken into account; that is, the shape that was measured by the reference image was omitted from the results. A similar approach was used for extracting the dent depth; the same extracting settings were used for all images so that a fair comparison could be made.

3.1 | Influence of shaking frequency

The effect of shaking frequency is investigated by imposing a sinusoidal acceleration $a(t)$ of constant amplitude $A_0 = 0.125$ g onto the modified DIC rig at different frequencies. Exposure time, t_{sh}, is fixed, while camera velocity amplitude, V_0, and motion-blur amplitude, w, vary according to Equation 1.[23,24]

$$\begin{cases} a(t) = \mathrm{Re}\left\{A_0 \cdot e^{j\omega t}\right\} \\ V_0 = \dfrac{A_0}{\omega} \\ w \propto V_0 \cdot t_{sh} \propto \dfrac{A_0}{\omega} \cdot t_{sh} \end{cases} \tag{1}$$

A frequency range of 5–20 Hz was set, with steps of 2.5 Hz. Consequently, as frequency increases, motion blur is expected to decrease together with uncertainty.[9] By comparing the measurements at different frequencies with the static test, it is clear that no bias is introduced by increasing shaking frequency, as indicated in Figure 8 in red. These data also revealed that no significant change in uncertainty is noticed under constant acceleration, which is indicated in blue on the same graph (using the scale on the right-hand side). This result is not consistent with the model in Equation 1 (even though a discontinuous decreasing trend can be seen in Figure 8). The reason is that by changing the shaking frequency, also the dynamic stiffness of the camera support is altered, resulting in a slight increase of camera relative motion as frequency changes. Hence, this phenomenon increases the measurement uncertainty, partially counteracting the decreasing trend due to motion blur. In the next paragraph, a constant frequency experiment will validate the hypothesis formulated in Equation 1.

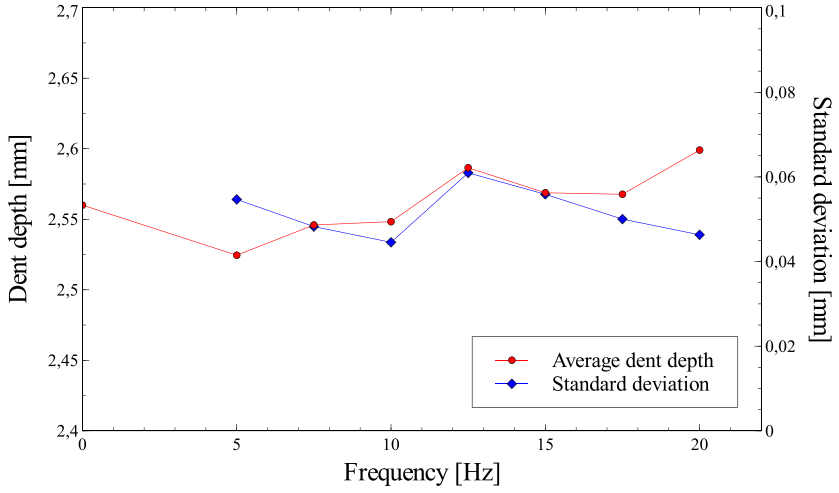

FIGURE 8 Average dent depth of Dent 4 and uncertainty (of 50 repetitions on Dent 4) versus shaker frequency-constant acceleration

3.2 | Influence of shaker acceleration

The effect of the shaker acceleration is investigated by setting the shaker frequency to a constant value of 5 Hz and varying the acceleration from 0.05 to 0.25 g in steps of 0.05 g. Considering Equation 1, motion blur is expected to increase linearly with amplitude. Consequently, uncertainty is expected to rise with a monotonically increasing trend. Figure 9 indicates that the measurements are becoming less accurate with increasing acceleration, which is probably caused by motion blur due to the higher acceleration. Note that the shaker frequency is constant during this test, removing the problem of the changing dynamic stiffness of the camera mount.

4 | INFLUENCE ON STRAIN MEASUREMENTS

A second series of tests were performed with a rubber specimen so that the influence of the camera vibration on strain measurements could be identified. This specimen (depicted in Figure 10) was introduced in Lava, Coppieters, Van Hecke, Van Houtte, and Debruyne (2012),[25] and it is loaded with a custom-made tensile machine in a vertical direction with a line load on the bottom side as indicated in Figure 10. The speckle pattern is painted directly on the specimen surface. Consequently, it is rigidly attached to the measured surface. In this way, even if the camera system moves, it is possible to grant both space and time matching for the strain computation (with respect to a static image of the unloaded specimen). The specimen has been chosen since it offers an heterogeneous strain state and different data extraction locations with high strain variations, while also being portable due to the custom setup (this is needed since the shaker used to vibrate the cameras cannot be moved due to the damping mass to which it is fixed). The same

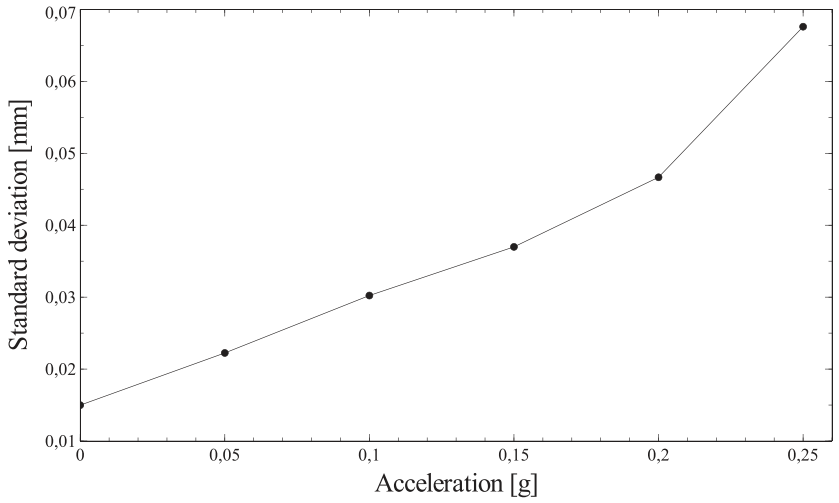

FIGURE 9 Dent identification uncertainty versus shaker acceleration-constant frequency

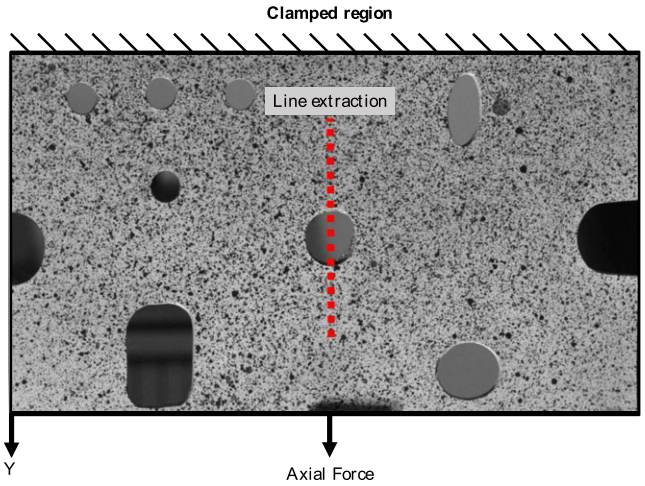

FIGURE 10 Rubber test specimen introduced in in Lava, Coppieters, Van Hecke, Van Houtte, and Debruyne (2012)[25] with vertical line extraction. The top line indicates the fixed upper border of the specimen, while the specimen is uniformly loaded at the bottom side

TABLE 4 Digital image correlation properties for the strain measurements

Parameter	Value
Camera resolution, pixels	1624 × 1234
Field of view, mm	200 × 150
Average speckle size, pixels	6
Exposure time,μs	12,500
Camera noise level, % dynamic range	0.5
Subset size, pixels	23
Step, pixels	4
Strain window size, pixels	5
Interpolation	B spline
Transformation	Affine

procedure for analysing the images was followed as in the previous section; the same reference image (now of the unloaded specimen) is used for analysing all data, and the input file system (batch-mode system of MatchID that provides the DIC processing parameters as a text file) was used, so data evaluation was done at the exact same pixels. The given DIC settings are given in Table 4 (with the strain window being the number of data points used for calculating the strain).

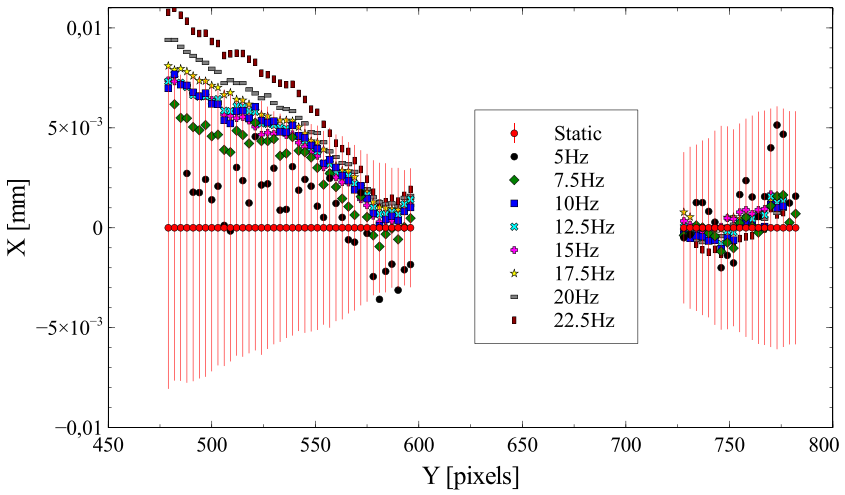

FIGURE 11 X coordinate of the shape measurement in the vertical line extraction. All data are subtracted by the data of the static test to clearly indicate the difference. The vertical red lines indicate the uncertainty of the static data

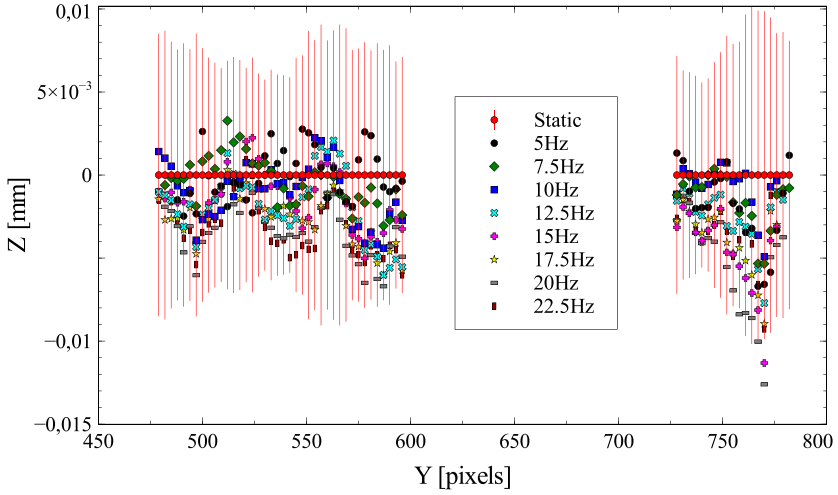

FIGURE 12 Out-of-plane shape component in the vertical line extraction. All data are subtracted by the data of the static test to clearly indicate the difference. The vertical red lines indicate the uncertainty of the static data

4.1 | Influence of shaker frequency

The effect of the shaker frequency is evaluated in this section by imposing a frequency range from 5 to 22.5 Hz in steps of 2.5 Hz, with a constant acceleration of 0.125 g. Images are again taken at random intervals, and a vertical line extraction (as indicated in Figure 10) is performed on all data after removing rigid-body motion. The horizontal in-plane component is depicted for all frequencies in Figure 11. All data are subtracted by the data of the static test to clearly indicate the difference between tests. The vertical red lines indicate the uncertainty in the static test, and from this, it is clear that there is a bias in the in-plane component, which increases with increasing frequency. This bias is not present in the out-of-plane component (as can be seen in Figure 12), which can be explained by the higher uncertainty in the out-of-plane component (as previously indicated in Balcaen, Reu, Lava, & Debruyne[26]) and the small order of magnitude of the bias.

The in-plane bias can be visualised by averaging the difference between the static and the shaking value for all pixels. This is shown in Figures 13 and 14 for the horizontal and vertical components, respectively, indicating a logarithmic behaviour for both and leading to a bias of 7.5 μm in X and 200 μm in Y.

The same logarithmic behaviour can be seen in the horizontal (Figure 15) and vertical (Figure 16) strain components, leading to errors up to 4,500 microstrain. This trend is probably caused by a low amount of motion blur that is present in the images due to the shaker and the finite exposure time of the cameras needed to acquire the image. This is further investigated by simulating a simple tensile experiment and by imposing different levels of motion blur in the next section.

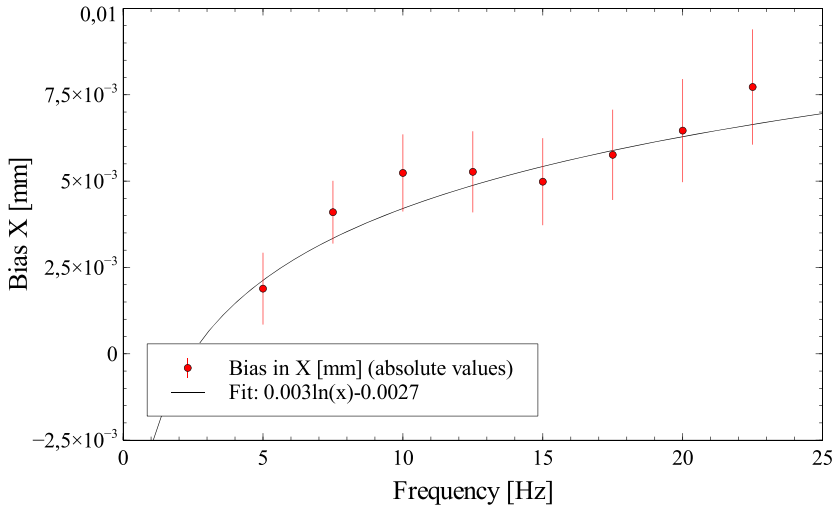

FIGURE 13 Frequency versus horizontal shape bias

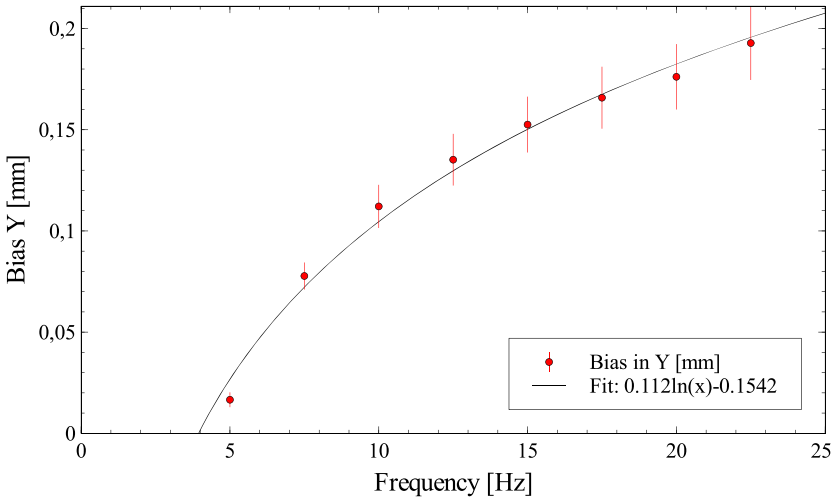

FIGURE 14 Frequency versus vertical shape bias

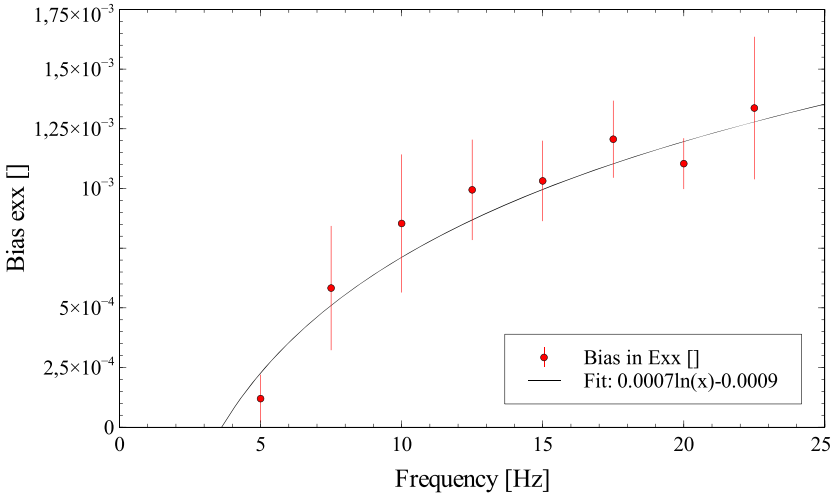

FIGURE 15 Frequency versus horizontal strain bias

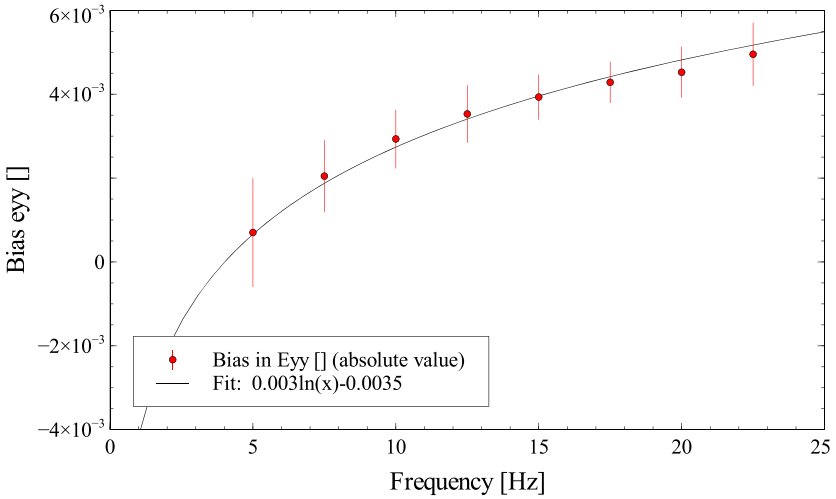

FIGURE 16 Frequency versus vertical strain bias

5 | MOTION BLUR AND THE INDUCED BIAS IN STEREO-DIC

Motion blur potentially induced a bias in the experimental data set, leading to the curves in Figures 13–16. Note that motion blur can have a more directional effect compared with regular defocus of the cameras, which (in the case of a low amount of defocus) can actually improve the results since the interpolation bias is reduced.[27,28] This is verified

by simulating a stereo-DIC experiment and by adding different levels of motion blur. The method for generating synthetic stereo-DIC images was previously published as in Balcaen, Wittevrongel, Reu, Lava, and Debruyne[29] but with no mention of motion blur. The process of adding motion blur is introduced here to the reader, and images of a uniform strained specimen are generated with different levels of motion blur so that its effect on strain identification can be studied.

5.1 | Imposing motion blur

The objective of applying motion blur onto an image is imposing a suitable degradation function, which leads to an effect that is similar to what happens when a finite exposure time is present together with a moving scene. This degradation function can be imposed by convoluting the reference image with a suitable kernel, as explained by Potmesil et al. in Potmesil and Chakravarty (1983).[30] The input image is defined as $f(x,y)$ and the motion-blurred output image as $g(x^{''}, y^{''})$. If a suitable convolution filter $h(x^{'},y^{'})$ is used as a point spread function, one can generate the blurred image as follows:

$$g(x,\mathrm{y}) = h\left(x^{'},y^{'}\right)*f(x,y), \tag{2}$$

in which the * indicates the convolution operation. Thanks to the property of Fourier transform. This convolution can be turned into a point-wise multiplication of spectra in the Fourier domain as follows:

$$G(x,\mathrm{y}) = H\left(x^{'},y^{'}\right)\cdot F(x,y), \tag{3}$$

where $F(x,y)$ is the spectrum of the reference image and $H(x^{'},y^{'})$ represents the optical transfer function (OTF). Since it is assumed that the entire field of view has the same amount of motion blur, a space invariant OTF (being a 2D *sinc* function defined by the magnitude and orientation of motion blur) can be employed, and the process is summarised as follows:

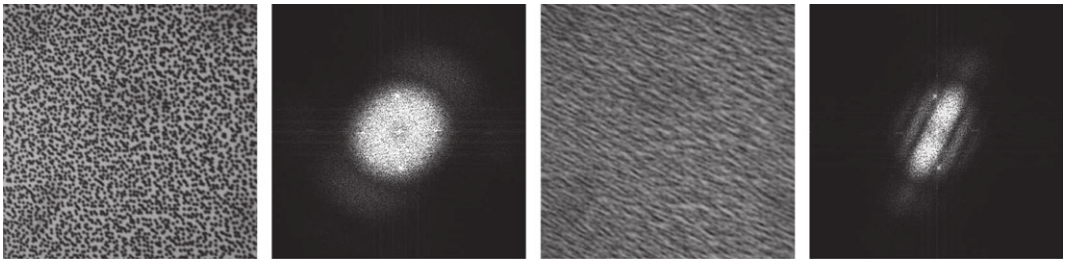

(a) Reference image (b) FT of the reference image (c) Motion blurred image (d) FT of the blurred image

FIGURE 17 Motion-blur image transformation

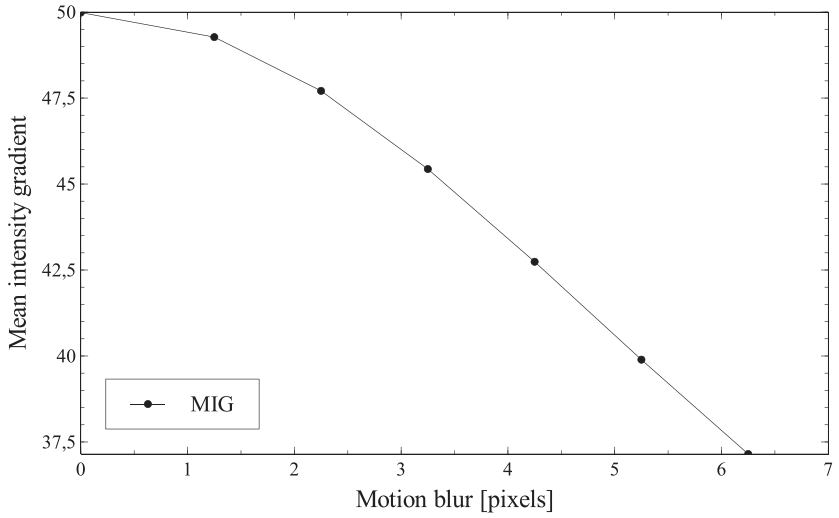

FIGURE 18 Mean intensity gradient vs. motion blur

1 Calculate the spectrum of the reference image by means of 2D fast Fourier transform (FFT).
2 Perform a multiplication of the spectrum of the reference image with the space invariant OTF.
3 Calculate the inverse Fourier transform of the convoluted image.

The effect of motion blur on the frequency content contained in the image is indicated in Figure 17a–d by giving motion-blurred images and their respective FFT (as earlier indicated in Lavatelli, 2015[31]). The FFT plots the magnitude component of the image versus the frequency (with a frequency of 0 Hz in the centre of the image and a white colour indicating a high magnitude). Figure 17a,b indicates the reference image and its respective FFT. The FFT clearly indicates a wide circular pattern, revealing a high power density. A heavily motion-blurred image is depicted in Figure 17c, together with its FFT in Figure 17d. A clear loss of high frequency content is noticeable, and the effect of the convolution process is visible as the banding in the FFT.[32] From Figure 17d, it is concluded that motion blur acts as a directional low-pass filter oriented accordingly with motion, thus reducing the frequency content of the image, which might lead to errors in the DIC routine. DIC is, namely, based on high image gradients (hence, the mean intensity gradient, abbreviated as MIG,[33] as a formulation for speckle quality), and a reduction in the frequency spectrum of the image degrades the magnitude of gradients. Eventually, this effect may lead to a degradation in correlation quality, as demonstrated in Zappa, Mazzoleni, and Matinmanesh (2014).[34]

5.2 | Influence of motion blur on strain identification

The influence of motion blur is investigated by generating images of a uniformly stretched specimen in which the deformed state is simulated with different levels of motion blur in the direction of the strain and perpendicular to the strain. The different deformed states are correlated with the same reference image, and the resulting Von Mises strain, epipolar distance, and the confidence interval sigma (indicating the variance of the displacement) is reported.

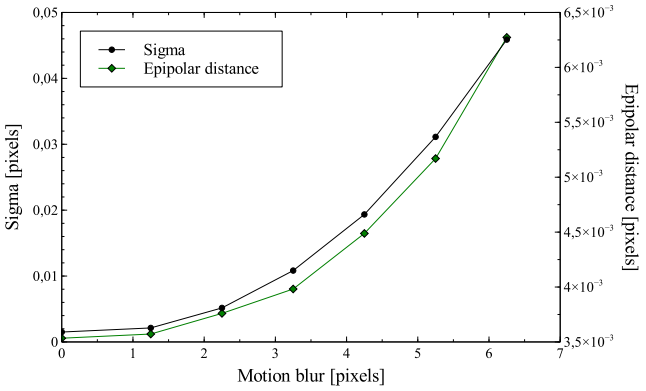

FIGURE 19 Confidence interval sigma and epipolar distance vs. motion blur

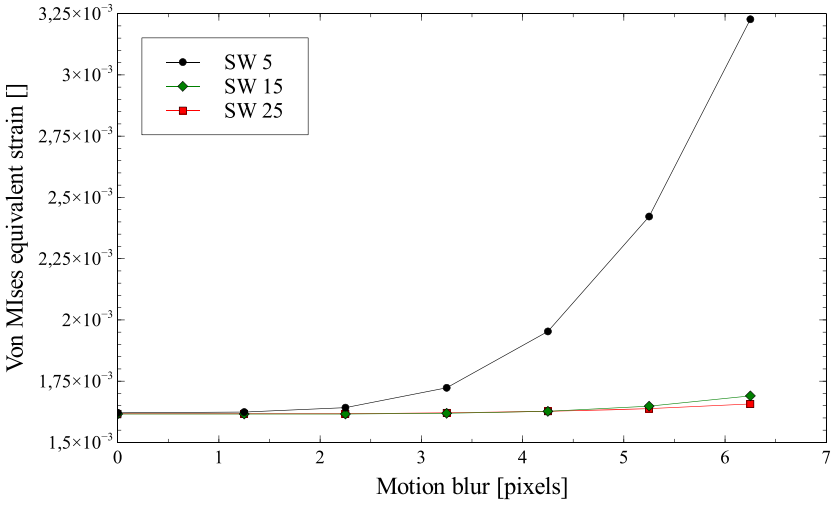

FIGURE 20 Equivalent Von Mises strain vs. motion blur

It is clear that a higher amount of motion blur results in a drop in the MIG value (see Figure 18), indicating a lower speckle quality. Figure 19 depicts the epipolar distance and the confidence interval sigma, which both rise at the same rate as the MIG drops. This results in a reduction of the accuracy, leading to a strain bias at lower virtual strain gauges (VSGs). Higher VSGs smooth the displacement field, thus reducing the bias, which is indicated in Figure 20 by the lower bias with increasing strain window size. There is also a small directional effect; the bias is slightly larger in the direction of the motion blur.

6 | CONCLUSION

In this work, the feasibility of installing a DIC rig on a quadcopter is evaluated by experimentally obtaining the vibration spectrum and by imposing it on a controlled setup. The effect of a shaking DIC rig on the uncertainty and bias of shape and strain measurements are evaluated by mounting a DIC setup on an electromagnetic shaker and vibrating the rig at different amplitudes and frequencies. Data was acquired during a stable hovering motion of a quadcopter, and an FFT was performed in order to ascertain the frequency and amplitude range to be imposed on the rig. Initial evaluation of the calibration parameters revealed a camera motion issue, so the rig was adapted with the focus on counteracting camera motion by bolting the cameras onto a stiff aluminium profile. The modified rig was first used for evaluating the depth of dents on a fuselage panel. By using the same reference image for all tests and by using a batch-mode system, data were evaluated at the same pixel locations. It was noted that there is no bias nor change in uncertainty at changing shaking frequencies and constant accelerations when measuring different dent depths. A decrease in uncertainty of up to 50 μm at 0.25 g is however present at higher accelerations, probably mainly due to motion blur in the images.

A second series of tests focussed on measuring strains in a perforated rubber specimen that was loaded with a custom-made tensile device (the test was earlier introduced in Lava, Coppieters, Van Hecke, Van Houtte, & Debruyne, 2012[25]). Displacements and strains were evaluated on a vertical line extraction through the central hole. The data indicated that there is a bias in the in-plane X and Y directions, while no noticeable bias is present in the out-of-plane direction, which can be explained by the higher accuracy in the in-plane components, making a small bias visible, while the low out-of-plane accuracy masks a small possible bias. A clear bias is present when evaluating strains; higher shaking frequencies induce higher biases (which follow a logarithmic trend). It can be concluded that a DIC system on a drone can only be feasible when measuring shapes, for example, dents in fuselage panels, while strain measurements are less feasible due to the frequency-induced bias, which can rise up to 4,500 microstrain at higher frequencies.

Lastly, the effect of motion blur on the strain accuracy is investigated. It is clear that higher amounts of motion blur reduce the frequency spectrum embedded in the image when the FFT plot is analysed. A reduced spectrum results in a lower mean intensity gradient, indicating a lower quality speckle pattern, which results in a lower correlation quality. The decreasing accuracy with higher accelerations can probably be reduced by using the optimised patterns, which can minimise the effect of motion blur. Optimised patterns will probably yield lower errors in the future, while external effects (e.g., wind gusts) will probably increase the error in the system.

ORCID

R. Balcaen http://orcid.org/0000-0002-6877-2459

REFERENCES

[1] M. A. Sutton, J. J. Orteu, H. W. Schreier, *Image correlation for shape, motion and deformation measurements*, Springer Science **2009**.

[2] B. Pan, K. Qian, H. Xie, A. Asundi, *Measurement Science and Technology* **April 2009**, *20*(6). 062001

[3] M. Rossi, F. Pierron, *Int. J. Solids Struct.* **February 2012**, *49*(3–4), 420.

[4] M. Bornert, F. Brémand, P. Doumalin, J.-C. Dupré, M. Fazzini, M. Grédiac, F. Hild, S. Mistou, J. Molimard, J.-J. Orteu, L. Robert, Y. Surrel, P. Vacher, B. Wattrisse, *Experimental Mechanics* **Jun 2009**, *49*(3), 353.

[5] Y. Q. Wang, M. A. Sutton, X. D. Ke, H. W. Schreier, P. L. Reu, T. J. Miller, *Experimental Mechanics* **April 2011**, *51*(4), 405.

[6] X. D. Ke, H. W. Schreier, M. A. Sutton, Y. Q. Wang, *Experimental Mechanics* **April 2011**, *51*(4), 423.

[7] https://www.dantecdynamics.com/q-480-handheld-dic-for-point-and-shoot-displacement-strain-measurement.

[8] Miller T. J., Schreier H. W., and Reu P. L. In *SEM annual Conf.*, **2007**.

[9] E. Zappa, A. Matinmanesh, P. Mazzoleni, *Opt. Lasers Eng.* **2014**, *59*, 82.

[10] M. Qinwai, M. Shaopeng, *Opt. Express* **2013**, *21*(6), 7686.

[11] D. Reagan, A. Sabato, C. Niezrecki, *Structural Health Monitoring* . 0(0):1475921717735326, 0

[12] G. D. Padfield, *Helicopter flight dynamics: The theory and application of flying qualities and simulation modelling*. AIAA education series, Wiley **2008**.

[13] M Morduchow and F. G. Hinchey. Technical Report v. 2218–2231, NACA - National Advisory Committee for Aeronautics, December 1950.

[14] https://github.com/cleanflight/blackbox-log-viewer.

[15] T. Hentschel, G. Fettweis, *IEEE Communications Magazine* **Aug 2000**, *38*(8), 142.

[16] http://www.dataphysics.com/.

[17] http://www.3ds.com/products-services/simulia/products/abaqus/.

[18] R. Balcaen, P. L. Reu, P. Lava, D. Debruyne, Submitted to*Experimental Mechanics* **2017**, *58*(7), 1101.

[19] P. L. Reu, *Experimental Mechanics* **November 2013**, *53*(9), 1661.

[20] C. Seher, M. Siegel, and W. M Kaufman. In Fourth Annual IEEE DualUse Technologies and Applications Conf., **1994**.

[21] I. Jovancevic, H.-H. Pham, R. Orteu, J.J. Gilblas, J. Harvent, X. Maurice, and L. Brèthes. *Journal of Nondestructive Evaluation*, *36*(46), **2017**.

[22] Cornelis Guijt, Daniel Hill, Justin Rausch, and Scott Fawaz. In *ICAF Conf.*, **2005**.

[23] A. Lavatelli, E. Zappa, *IEEE Trans. Instrum. Meas.* **Aug 2016**, *65*(8), 1818.

[24] A. Lavatelli, E. Zappa, *IEEE Trans. Instrum. Meas.* **March 2017**, *66*(3), 451.

[25] P. Lava, S. Coppieters, R. Van Hecke, P. Van Houtte, D. Debruyne, *Experimental Techniques* **2012**, *37*(4), 72.

[26] R. Balcaen, P. L. Reu, P. Lava, D. Debruyne, *Experimental Mechanics* **2017**, *57*, 939.

[27] J. C. Passieux, P. Navarro, S. Marguet, J.-F. Ferrero, *Experimental Mechanics* **2014**, *54*(8), 1453.

[28] A. Charbal, J. Dufour, A. Guery, F. Hild, L. Vincent, S. Roux, M. Poncelet, *Optics and Lasers in Engineering* **2016**, *78*, 75.

[29] R. Balcaen, L. Wittevrongel, P. L. Reu, P. Lava, D. Debruyne, *Experimental Mechanics* **2017**, *57*(5), 703.

[30] M. Potmesil, I. Chakravarty, *Computer Graphics* **1983**, *17*(3), 389.

[31] A. Lavatelli. Master's thesis, Politecnico di Milano, Italy, **2015**.

[32] J. Zhang, F. He, W. Li, *Motion blurring direction identification based on second-order difference spectrum*, pages 102–109, Springer Berlin Heidelberg, Berlin, Heidelberg **2011**.

[33] B. Pan, Z. Lu, H. Xie, *Opt. Lasers Eng.* **April 2010**, *48*(4), 469.

[34] E. Zappa, P. Mazzoleni, A. Matinmanesh, *Opt. Lasers Eng.* **2014**, *56*, 140.

How to cite this article: Balcaen R, Lavatelli A, Jiménez-Peña C, Pfeiffer H, Zappa E, Debruyne D. Impact of motion blur on stereo-digital image correlation with the focus on a drone-carried stereo rig. *Strain*. 2019;55: e12300. https://doi.org/10.1111/str.12300